A&A manuscript no.
(will be inserted by hand later)

Your thesaurus codes are:
10 (02.14.1 09.01.1, 10.01.1, 10.08.1)

ASTRONOMY AND ASTROPHYSICS

Metal-poor halo stars as tracers of ISM mixing processes during halo formation

D. Argast[1,2], M. Samland[1], O. E. Gerhard[1] and F.-K. Thielemann[2]

[1] Astronomisches Institut der Universität Basel, Venusstrasse 7, CH-4102 Binningen, Switzerland (argast@astro.unibas.ch)
[2] Institut für Physik der Universität Basel, Klingelbergstrasse 82, CH-4056 Basel, Switzerland (fkt@quasar.physik.unibas.ch)

Received ..., accepted ...

Abstract. We introduce a stochastic halo formation model to compute the early chemical enrichment of the interstellar medium (ISM) of the halo. Contrary to 1-zone chemical evolution models, we are able to resolve local inhomogeneities in the ISM caused by single core-collapse supernovae. These inhomogeneities lead to different element abundance patterns in very metal-poor stars, which can be seen as scatter in the abundances of halo stars with metallicities [Fe/H] < 2.0.

The early chemical evolution of the halo proceeds in different enrichment phases: At [Fe/H] < -3.0, the halo ISM is unmixed and dominated by local inhomogeneities caused by individual core-collapse supernova (SN) events. For metallicities [Fe/H] > -2.0 the halo ISM is well mixed, showing an element abundance pattern integrated over the initial mass function. In the range $-3.0 <$ [Fe/H] < -2.0 a continuous transition from the unmixed to the well mixed ISM occurs.

For some elements (Si, Ca, Eu), the scatter in the element-to-iron ratio [El/Fe] of metal-poor halo stars can be reproduced. Stellar yields of other elements predict a scatter which, compared to the observations, is too large (O, Mg) or too small (Ni). Cr and Mn show a decreasing trend for lower metallicities, which can not be explained by metallicity independent yields, provided that the mixing of the ejecta with the interstellar medium does not depend on progenitor mass. This demonstrates the need for revised, self-consistent SN yields.

Finally, we discuss the metallicity distribution in the model. Compared to the 28 very metal-poor stars observed with metallicities in the range $-4.0 <$ [Fe/H] < -3.0, no star is known with confirmed metallicity [Fe/H] < -4.0, while our model predicts 5 ± 2 stars with [Fe/H] < -4.0. These should be present if the halo ISM started at primordial metallicities and no pre-enrichment by population III stars occurred.

Key words: ISM: abundances – Physical processes: Nucleosynthesis – Galaxy: abundances – Galaxy: halo

1. Introduction

The low metal abundances and high peculiar velocities of halo stars indicate that the halo is an old, if not the oldest component of the Milky Way. Age determinations of globular clusters and halo field stars point to an age of 14-15 billion years with no detectable age gradient with galactocentric distance (Harris et al. 1997). The halo has therefore special significance for the formation of the Milky Way. There are two quantities which play important rôles in the investigation of the formation of the halo: the orbits of halo stars and their chemical composition. Since halo stars form a collisionless system, their orbits contain information about the dynamics at the time of star formation and thus the formation of the halo (e.g. Carney et al. 1996; Chiba & Yoshii 1998). Information about the chemical composition of the interstellar medium (ISM) of the halo is more direct. The element abundances observed in low mass halo stars directly reflect the chemical abundances and the chemical inhomogeneity of the ISM during halo formation (McWilliam 1997).

Examinations of element abundance ratios as function of metallicity [Fe/H] show that star-to-star differences rise with decreasing metallicity (Ryan et al. 1996). Most of the chemical elements are ejected during supernovae Type II (SNe II) explosions. The enrichment of the halo depends on how many SNe II explode and how effectively the ejected gas is mixed with the surrounding ISM. If the ejected metals are distributed over a large volume, a spatially homogeneous enrichment takes place. If the mixing volume is small, the ISM in the vicinity of a core-collapse supernova (SN II) is highly enriched, while large parts of the halo gas remain metal-poor. In this case the ISM is chemically highly inhomogeneous and newly formed stars are of different chemical composition, depending on where they form. In this scenario one should moreover expect that the metal-poorest stars have chemical compositions corresponding to the stellar yields of single SNe II (Ryan et al. 1996).

In this paper we present a stochastic chemical evolution model and investigate the inhomogeneous enrichment of the halo ISM. The description of the model is given in Sect. 2, followed by an overview of theoretical SN II yields and their uncertainties in Sect. 3. The employed observational data is presented in Sect. 4. The results of our model and the conclusions are given in Sect. 5 and 6, respectively.

2. The Model

Very metal-poor halo stars show a great diversity in their element abundances and therefore a scatter in their element-

to-iron ratios [El/Fe] of order 1 dex. This scatter gradually decreases at higher metallicities until a mean element abundance is reached which corresponds to the [El/Fe] ratio of the stellar yields integrated over the initial mass function (IMF). The aim of our stochastic halo formation model is to understand the trends seen in the observations and to investigate how the metal-poor interstellar medium (ISM) in the halo evolves chemically.

Our fully 3D-code, contrary to 1-zone chemical evolution models, enables us to resolve local inhomogeneities in the ISM with a spatial resolution of 50 pc. All in all, we model a volume of (2.5 kpc)^3, divided into 50^3 cells. Every cell of our grid contains detailed information about the enclosed ISM and the mass distribution of stars. We consider simultaneously the evolution of nine elements, the α-elements O, Mg, Si and Ca, the iron-peak elements Cr, Mn, Fe and Ni and the r-process element Eu.

Our initial conditions assume a halo ISM consisting of a homogeneously distributed single gas phase with primordial abundances and a density of 0.25 particles per cm^3, which gives a total mass of about $10^8\,\mathrm{M}_\odot$ in a volume of (2.5 kpc)^3. We adopt a constant time-step of 10^6 years since it has to be longer than the dynamical evolution of a supernova (SN) remnant and shorter than the lifetime of the most massive stars. At each time-step 20 000 cells are chosen randomly and independently of each other and of the state of the enclosed ISM. Each selected cell may create a star with a probability proportional to the square of the local ISM density (Larson 1988). The number of stars formed per time-step is the product of the number of cells tested with the probability of star formation in each cell. Various combinations of these parameters are possible to achieve a given SFR; the choice of 20 000 cells proved computationally convenient. The absolute value of the SFR influences the *time-scale* of the enrichment process (cf. Sect. 5.1), but *not* the evolution of [El/Fe]-ratios as function of [Fe/H]. Therefore, the main results of this paper are insensitive to the values of these parameters.

The mass of a newly formed star is chosen randomly from a Salpeter IMF. The lower and upper mass limits of the IMF are taken to be $0.1\,\mathrm{M}_\odot$ and $50\,\mathrm{M}_\odot$, respectively. About 5000 stars are formed on average during each step. Newly born stars inherit the abundance pattern of the ISM out of which they form, carrying therefore information about the state of the ISM at the place and time of their birth. To determine the lifetime of a star an approximation to the metallicity dependent mass-lifetime relation of the *Geneva Stellar Evolution and Nucleosynthesis Group* (cf. Schaller et al. 1992; Schaerer et al. 1993a; Schaerer et al. 1993b; Charbonnel et al. 1993) is used, given by

$$\log(T) = (3.79 + 0.24 \cdot Z) - (3.10 + 0.35 \cdot Z)\,\log(M) + (0.74 + 0.11 \cdot Z)\,\log^2(M),$$

where T is the lifetime in units of 10^6 yr, Z the metallicity in units of solar metallicity $Z_\odot$ and M the mass in units of solar masses $\mathrm{M}_\odot$.

Stars in a range of $10 - 50\,\mathrm{M}_\odot$ will explode as core-collapse supernovae (SNe II), resulting in an enrichment of the neighbouring ISM. Stellar yields are taken from Thielemann et al. (1996) and Nomoto et al. (1997) for all elements except Eu. Since there are no theoretical predictions of stellar Eu yields, we use the indirectly deduced yields of Tsujimoto & Shigeyama (1998) which assume that r-process elements originate from SNe II (see the discussion of stellar yields in Sect. 3). We linearly interpolate the stellar yields given in these papers, since we use a finer mass-grid in our simulation. For SNe with masses below $13\,\mathrm{M}_\odot$ stellar yields are not available. Since the nucleosynthesis models show declining yields towards low progenitor masses, we have for the interpolation arbitrarily set the yields of a $10\,\mathrm{M}_\odot$ SN to one thousandth of those of a $13\,\mathrm{M}_\odot$ SN. The interpolation gives IMF averaged values of the [El/Fe] ratios, which are in good agreement with the observed mean values of metal-poor stars in all elements except Ca, which shows a [Ca/Fe] ratio that is about 0.3 dex lower than the observed mean. We do not include supernovae (SNe) of Type Ia, since we are only interested in the very early enrichment of the halo ISM, which is dominated by SNe of Type II.

Intermediate mass stars will evolve to planetary nebulae, returning only slightly enriched material in the course of their evolution. This locally influences the enrichment pattern of the gas, since metal-poor material is returned into the evolved and enriched ISM. It will not change the element abundances [El/H] significantly, but can affect the local element-to-iron ratios [El/Fe] considerably. Low mass stars do not evolve significantly during the considered time. In our model, they serve to lock up part of the gas mass, affecting therefore the local element abundances [El/H] in the ISM.

Since the explosion energy of a core-collapse supernova (SN II) depends only slightly on the mass of its progenitor (Woosley & Weaver 1995; Thielemann et al. 1996), every SN II sweeps up a constant mass of about $5 \times 10^4\,\mathrm{M}_\odot$ of gas (Ryan et al. 1996; Shigeyama & Tsujimoto 1998). In our model the radius of the SN remnant then is computed from the local density of the ISM and lies typically between 100 pc and 200 pc. The ejecta of the SN II and all the swept up, enriched material are condensed in a spherical shell which is assumed to be chemically well mixed. The material in the shell subsequently mixes with the ISM of the cells where the expansion of the remnant stopped. The interior of the remnant, where all the material was swept up, is assumed to be filled with about $5\,\mathrm{M}_\odot$ of dilute gas from the SN event with the corresponding metal abundances. This gas is unable to form stars until it is swept up by another SN event and mixed with the surrounding ISM. Thus this material contributes to the enrichment only after some delay.

The star formation rate of cells influenced by the remnant will rise, since their density is higher than the average density of a cell and the probability to form a star is assumed to be proportional to the square of the local density. It is still possible to form stars in the field, but cells that are influenced by a SN remnant are favoured. Stars which form out of material enriched by a single SN inherit its abundances and therefore show an abundance pattern which is characteristic for this particular progenitor mass. The most metal-poor stars that form out of material which was enriched by only one SN would therefore

allow to reconstruct the stellar yields of single core-collapse SN, if the average swept up mass and the absolute yield of one element were known (Shigeyama & Tsujimoto 1998).

The SN remnant expansion is the only dynamical process taken into account in our model. Therefore, this model has the least possible mixing of the ISM. This is the opposite limit as in the case of closed box models, which assume a complete mixing of the ISM at all times and are therefore not able to explain the scatter seen at low metallicities. We continue our calculation up to an averaged iron abundance of [Fe/H] $= -1.0$. At this metallicity SN events of Type Ia, which we have not included in our model, would start to influence the ISM.

3. SN II yields and their uncertainties

In the present investigation we make use of the nucleosynthesis results by Thielemann et al. (1996) and Nomoto et al. (1997). Here we want to give a short summary of the key features together with an assessment of the uncertainties by comparing with available independent calculations. The synthesized elements form three different classes which are sensitive to different aspects of the stellar models and supernovae explosion mechanism: (1) stellar evolution, (2) stellar evolution plus the explosion energy, and (3) details of the explosion mechanism which includes aspects of stellar evolution determining the size of the collapsing Fe-core. Due to reaction equilibria obtained in explosive burning, the results do not show a strong sensitivity to the applied reaction rate library (Hoffman et al. 1999).

1: The abundances of C, O, Ne, and Mg originate from the unaltered (essentially only hydrostatically processed) C-core and from explosive Ne/C-burning. They are mainly dependent on the structure and zone sizes of the pre-explosion models resulting from stellar evolution. These zones and therefore the amount of ejected mass varies strongly over the progenitor mass range. O, Ne, and Mg vary by a factor of 10-20 between a $13\,\mathrm{M}_\odot$ and a $25\,\mathrm{M}_\odot$ progenitor star. This behaviour can vary with the treatment of stellar evolution and is strongly related to the amount and method of mixing in unstable layers. Woosley & Weaver (1995) employ the Ledoux criterion with semiconvection for Schwarzschild-unstable but Ledoux-stable layers. Nomoto & Hashimoto (1988) make use of the Schwarzschild criterion for convection (neglecting composition gradients) which ensures mixing over more extended regions than the Ledoux criterion. The Schwarzschild criterion causes larger convective cores (see also Chieffi et al. 1998) which leads to larger ^{16}O, ^{20}Ne, and ^{24}Mg yields, the latter being also dependent on the $^{12}\mathrm{C}(\alpha,\gamma)$ rate (Langer & Henkel 1995). In addition, it is important to know the mixing velocity in unstable regions. Recent calculations by Umeda et al. (1999), within the diffusion approximation for mixing (Spruit 1992; Saio & Nomoto 1998) but with a remaining free parameter - permitted to vary between 0 and 1 - show that the Woosley & Weaver (1995) results can be reproduced with a small choice of this parameter of 0.05. A further effect is due to rotation. When also treating rotation correctly (Langer et al. 1997; Talon et al. 1997; Meynet & Maeder 1997; Heger et al. 1999), rotational instabilities lead to additional mixing which can bring the models making use of the Ledoux criterion closer to those evolved with the Schwarzschild criterion and the compositions closer to those obtained with instantaneous mixing (high mixing velocities). Thus, the amount of mixing (being influenced by the mixing criterion utilized, the mixing velocity, and rotation) determines in stellar evolution the size of the C/O core. While the yield of O can be fixed with a combination of the still uncertain $^{12}\mathrm{C}(\alpha,\gamma)$ rate (Buchmann 1996, 1997) and a mixing description, the yields of Ne and Mg depend on the extent of mixing. Recent galactic chemical (but not dynamic) evolution calculations (Thomas et al. 1998; Matteucci et al. 1999; Chiappini et al. 1999) prefer apparently a larger extent of mixing (caused by either of the effects mentioned above) in order to reproduce the observed Mg in low metallicity stars.

2: The amount of mass for the elements Si, S, Ar and Ca, originating from explosive O- and Si-burning, is almost the same for all massive stars in the Thielemann et al. (1996) models. They do not show the strong progenitor mass dependence of C, O, Ne, and Mg. Si has some contribution from hydrostatic burning and varies by a factor of 2-3. Thus, the first set of elements (C, O, Ne, Mg) tests the stellar progenitor models, while the second set (Si, S, Ar, Ca) tests the progenitor models and the explosion energy, because the amount of explosive burning depends on the structure of the model plus the energy of the shock wave which passes through it. Present models make use of an artificially induced shock wave via thermal energy deposition (Thielemann et al. 1996) or a piston (Woosley & Weaver 1995) with shock energies which lead, after the reduction of the gravitational binding of ejected matter, to a given kinetic energy. In our models this is an average energy of 10^{51} erg, known from remnant observations, which does not reflect possible explosion energy variations as a function of progenitor mass. The apparent underproduction of Ca seen in some chemical evolution calculations (e.g. Thomas et al. 1998; Matteucci et al. 1999; Chiappini et al. 1999) could apparently be solved by a progenitor mass dependent explosion mechanism and energy.

3: The amount of Fe-group nuclei ejected (which includes also one of the so-called alpha elements, i.e. Ti) and their relative composition depends directly on the explosion mechanism, connected also to the size of the collapsing Fe-core. Observational checks of individual supernovae are presently still required to test the detailed working of a supernova. The present situation is still uncertain and depends on Fe-cores from stellar evolution, the supranuclear equation of state and maximum neutron star mass, related to the total amount of gravitational binding energy release of the collapsed protoneutron star, the resulting total amount of neutrinos, and the time release (luminosity), dependent on neutrino transport via numerical treatment, convective transport, and opacities (Burrows 1990; Herant et al. 1994; Janka & Müller 1995, 1996; Keil & Janka 1995; Burrows et al. 1995, 1996; Reddy & Prakash 1997; Burrows & Sawyer 1998; Mezzacappa et al. 1998; Messer et al. 1998; Yamada et al. 1999; Pons et al. 1999). Three types of uncertainties are inherent in the Fe-group ejecta, related to (i) the

total amount of Fe (-group) nuclei ejected and the mass cut between neutron star and ejecta, mostly measured by ^{56}Ni decaying to ^{56}Fe, (ii) the total explosion energy which influences the entropy of the ejecta and with it the degree of alpha-rich freeze-out from explosive Si-burning and the abundances of radioactive ^{44}Ti as well as ^{48}Cr, the latter decaying later to ^{48}Ti and being responsible for elemental Ti, and (iii) finally the neutron richness or $Y_{\rm e}$=$< Z/A >$ of the ejecta, dependent on stellar structure and the delay time between collapse and explosion. $Y_{\rm e}$ influences strongly the ratios of isotopes 57/56 in Ni (Co, Fe) and the overall elemental Ni/Fe ratio. The latter being dominated by ^{58}Ni and ^{56}Fe. The position of the mass cut has also a side effect (besides determining the total amount of ^{56}Ni/Fe), it influences the ratio of abundances from alpha-rich freeze-out and incomplete Si-burning, affecting in this way the abundances of the elements Mn (^{55}Co decay), Cr (^{52}Fe decay) and Co (^{59}Cu decay) as discussed in Nakamura et al. (1999).

There is limited direct observational information from individual supernovae with known progenitors (SN 1987A, SN 1993J, 1997D?, 1996N?, 1994I) and possible hypernovae (SN1997ef, 1998bw), leading to direct O, Ti or Fe (Ni) observations (e.g. Shigeyama & Nomoto 1990; Iwamoto et al. 1994, 1998, 1999a, 1999b; Turatto et al. 1998; Sollerman et al. 1998; Kozma & Fransson 1998; Bouchet et al. 1991; Suntzeff et al. 1992). As explosive nucleosynthesis calculations cannot presently rely on self-consistent explosion models, the position of the mass cut is in all cases an assumption and has mostly been normalized to observations of SN 1987A. Whether there is a decline in Fe-ejecta as a function of progenitor mass (as assumed in Thielemann et al. 1996) or actually an increase (Woosley & Weaver 1995) or a more complex rise, maximum and decline (Nakamura et al. 1999) is not really understood. Thus, the results by Thielemann et al. (1996) utilized here are showing the correct IMF integrated behaviour of e.g. Si/Fe, but one has to keep in mind that e.g. O/Fe, Mg/Fe, Si/Fe, Ca/Fe yields of individual supernovae could be quite uncertain and even show an incorrect progenitor mass dependence or a larger scatter than (yet unknown) realistic models. Ratios within the Fe-group (like e.g. Ni/Fe) have been obtained by mass cut positions which reproduce the solar ratios. Thus, the theoretical yields might show already the average values and a much smaller scatter than some observations (see e.g. Henry 1984). Later work attempted to choose mass cuts in order to represent some specific element trends like e.g. in Cr/Fe, Co/Fe or Mn/Fe (Nakamura et al. 1999).

In general we should keep in mind that as long as the explosion mechanism is not completely and quantitatively understood yet, one has to assume a position of the mass cut. Dependent on that position, which is a function of explosion energy and the delay time between collapse and final explosion, the total amount of Fe-group matter can vary strongly, Ti-yields can vary strongly due to the attained explosion energy and entropy, and the ejected mass zones will have a variation in neutron excess which automatically changes relative abundances within the Fe-group, especially the Ni/Fe element ratio.

4: r-Process Yields. SNe II have long been expected to be the source of r-process elements. Some recent calculations seemed to be able to reproduce the solar r-process abundances well in the high entropy neutrino wind, emitted from the hot protoneutron star after the SN II explosion (Takahashi et al. 1994; Woosley et al. 1994). If the r-process originates from supernovae, a specific progenitor mass dependence has to be assumed in order to reproduce the r-process abundances in low metallicity stars as a function of [Fe/H] (Mathews et al. 1992; Wheeler et al. 1998). Such a "hypothetical" r-process yield curve has been constructed by Tsujimoto & Shigeyama (1998), in agreement with ideas of Ishimaru & Wanajo (1999) and Travaglio et al. (1999), and is used in the present galactic evolution calculation. However, we should keep in mind that present-day supernova models have difficulties to reproduce the entropies required for such abundance calculations. In addition, they could exhibit the incorrect abundance features of lighter r-process nuclei (Freiburghaus et al. 1999a), we know by now that at least two r-process sources have to contribute to the solar r-process abundances (Wasserburg et al. 1996; Cowan et al. 1999), and that possible other sources exist (Freiburghaus et al. 1999b). A larger scatter in the r/Fe ratio in low metallicity stars than predicted by the constructed supernova yields would also indicate the need of such another r-process source.

4. Observational Data

As shown in Table 1, the observational data were selected from various high-resolution studies. Elements marked with "c" were adjusted to the same solar abundance scale by S. G. Ryan (Ryan et al. 1996 and private communication), entries marked with "x" remained unaltered. Unmarked entries were not observed in the corresponding study. All observations of very metal-poor stars published after 1989 were taken into account. In the case where multiple observations of stars exist, we used the most recent data. If they were published in the same year or *after* 1995, the values were averaged.

Typical abundance errors given for these observations are about 0.1 dex (see Ryan et al. 1996). These may not fully account for systematic errors, which could, e.g., be caused by the choice of the employed stellar atmosphere models and parameters, or by the employed solar abundance values. If there are systematic offsets between different subsamples, this could enhance the scatter in the combined sample.

Special attention has to be paid to Cr, Mn and O. In the case of Cr and Mn, data published after 1995 show a decrease in the [Cr/Fe] and [Mn/Fe] ratios for lower metallicities. Such trends are not present in older observations. Regardless of this, it is not possible to reproduce metallicity-dependent trends with our model, since we only use the stellar yields of Thielemann et al. (1996), which assume constant solar progenitor star metallicity. A possible explanation of the [Cr/Fe] and [Mn/Fe] trends is the dependency of stellar yields on the metallicity of the progenitor star of a SN Type II (Samland 1997) or a progenitor mass dependent mixing of SN II yields with the ISM (Nakamura et al. 1999).

Table 1. Reference list of the observational data. Elements marked with "c" were adjusted to the same solar abundance scale by S. G. Ryan (Ryan et al. 1996 and private communication), unaltered observations are marked with "x". Unmarked entries were not observed in the corresponding study. Newer publications (after 1995) are listed separately.

Author	O	Mg	Si	Ca	Cr	Mn	Fe	Ni	Eu
Gratton (1989)						c	c		
Magain (1989)		c		c	c		c		x
Molaro & Bonifacio (1990)		c		c	c		c		
Molaro & Castelli (1990)		c	c	c	c	c	c	c	
Peterson et al. (1990)	x	c	c	c	c	c	c	c	
Zhao & Magain (1990)				c	c		c	c	
Bessell et al. (1991)	x						x		
Gratton & Sneden (1991a)			c	c	c		c	c	
Gratton & Sneden (1991b)							x		x
Ryan et al. (1991)	x	c	c	c	c	c	c	c	x
Spiesman & Wallerstein (1991)	x						x		
Spite & Spite (1991)	x						x		
Francois et al. (1993)							x		x
Norris et al. (1993)		c		c	c	c	c	c	
Beveridge & Sneden (1994)	x	x	x	x	x	x	x	x	x
King (1994)	x						x		
Nissen et al. (1994)	x	x		x	x		x		
Primas et al. (1994)		c	c	c	c	c	c		
Sneden et al. (1994)		x	x	x	x	x	x		x
Fuhrmann et al. (1995)	x						x		
McWilliam et al. (1995)		c	c	c	c	c	c	c	x
Balachandran & Carney (1996)	x						x		
Ryan et al. (1996)		c	c	c	c	c	c	c	c
Israelian et al. (1998)	x						x		
Jehin et al. (1999)		x		x	x		x	x	x

In the data set of Israelian et al. (1998), the [O/Fe] ratio increases at lower metallicities. This behaviour is apparently different from previous determinations and is not yet understood, but almost identical results were published by a different group of observers (Boesgaard et al. 1999). The α-elements oxygen and magnesium are produced mainly during the hydrostatic burning phase of a high mass star and are only slightly affected by the actual explosion. Furthermore, their yields depend in almost the same way on the mass of the progenitor star (Thielemann et al. 1996; Woosley & Weaver 1995). Thus observations of Mg for the objects discussed in the O abundance determinations by Israelian et al. (1998) and Boesgaard et al. (1999) would be very interesting.

5. Results

5.1. Chemical Mixing of the Halo ISM

Starting with an ISM of primordial abundances, a first generation of ultra metal-poor stars is formed in the model. After the first high-mass stars exploded as SNe of Type II, the halo ISM is dominated by local inhomogeneities, since the SN events are spatially well separated and no mixing has yet occurred. In a very metal-poor medium, a single SN event heavily influences its surroundings, so that its remnant shows the element abundance pattern produced by that particular core-collapse SN. Stars born out of this enriched material therefore inherit the same abundances. Since SNe of different progenitor masses have different stellar yields, stars formed out of an incompletely mixed ISM show a great diversity in their element abundances.

Fig. 1 shows a cut through the computed volume, giving the density distribution of the halo ISM at four different times, ranging from the unmixed to the well mixed stage. Each panel shows a different mean metallicity and has a lateral length of 2.5 kpc. The density of the ISM ranges from $6 \cdot 10^{-7}\,\mathrm{M}_{\odot}/pc^3$ in the inner part of a remnant to $0.04\,\mathrm{M}_{\odot}/pc^3$ in the densest clouds, which is about the gas density of the solar neighbourhood (Binney & Tremaine 1987).

Upper left: After 82 Myr (see below for the scaling of the time units with the assumed SFR), the mean metallicity of the halo ISM is [Fe/H] $= -3.5$. Most of the volume was not yet affected by SN events, which can be seen as bright patches in the otherwise homogeneously distributed ISM. In the inner part of the remnants most of the gas has been swept up and condensed in thin shells, which show up as dark, ring-like structures. The regions influenced are well separated and no or only slight mixing on a local scale has taken place. The halo ISM has to be considered unmixed and is dominated by local inhomogeneities. Stars forming in the neighbourhood of such inho-

mogeneities show an abundance pattern which is determined by the ejecta of a single SN or a mixture of at most two to three SN events.

Upper right: Beginning of the transition from the unmixed to the well mixed halo ISM, after 170 Myr at a mean metallicity of [Fe/H] $= -3.0$. The separation of single SN remnants has become smaller and a higher number of remnants may overlap. The abundance pattern in overlapping shells still shows a great diversity but is closer to the IMF averaged element abundance than at the completely unmixed stage.

Lower left: After 430 Myr, at a mean metallicity of [Fe/H] $= -2.5$, enough SN events have occurred to pollute the mass of the whole ISM twice. Nevertheless there are still cells which were not influenced by a S, showing therefore primordial abundances.

Lower right: After 1430 Myr, a mean metallicity of [Fe/H] $= -2.0$ is reached. At this time, no patches with primordial abundances exist and the ISM starts to be chemically well mixed. The once homogeneous, primordial medium has now a lumpy structure with large density fluctuations and shows mainly an IMF averaged abundance pattern.

Our calculations confirm that the incomplete mixing of the ISM during the halo formation plays a significant rôle in the early enrichment of the metal-poor gas. This can be seen in the [El/Fe] ratios of the considered elements, shown in Fig. 2. The small, filled squares show the [El/Fe] ratio of single model-stars. For comparison, observed metal-poor stars are represented by open squares. In the case of O, Cr and Mn, observations taken before 1995 were marked with open triangles. This was done to highlight possible trends in the [El/Fe] ratio of these elements. If multiple observations of a metal-poor star occurred and the abundances had to be averaged, open diamonds were used (see Sect. 4 for details).

The numbered circles show the [El/Fe] and [Fe/H] ratios of a single SN II with the indicated mass. The [Fe/H] ratio in the shell of the SN remnants are determined by the mass of the exploding star and the $5 \times 10^4\,\mathrm{M}_\odot$ of gas that are swept up by the shock front. This ratio represents the maximal abundance a *single* SN II can produce and determines the position of the open circles on the [Fe/H] axis in Fig. 2. If the swept up material subsequently mixes with the surrounding medium, this abundance decreases and stars with lower [Fe/H] abundance can be formed. On the other hand, the [El/Fe] ratio is determined solely by the stellar yields of a SN II and is independent of the mixing mass. For the uncertainties of Fe-ejecta and [El/Fe] ratios in individual SNe II see the discussion in Sect. 3.

We divide the chemical enrichment process in the early evolution of the halo ISM into different enrichment stages: at metallicities [Fe/H] < -3.0, the ISM is completely unmixed and dominated by local inhomogeneities, originating from SN II events. At about [Fe/H] > -2.0 the halo ISM shows an IMF averaged abundance pattern and has to be considered chemically well mixed. The continuous transition between these two phases is marked by incomplete mixing which gradually becomes better, as more and more high-mass stars explode as SN II.

The different phases in the enrichment of the halo ISM seen in Fig. 2 can be distinguished in all [El/Fe] – [Fe/H] plots. At very low metallicities ([Fe/H] < -3.0), only a few stars exist, showing a considerable spread in their [El/Fe] ratios, ranging from 0.5 dex in the case of Ni to more than 2 dex in the cases of O, Mg and Eu. At this stage, the scatter of the model stars is given by the spread in metallicities of the SN models. At the end of this early phase, less than 0.5% of the total halo ISM mass has been transformed into stars.

At a metallicity of $-3.0 <$ [Fe/H] < -2.0, the SN remnants start to overlap and a first, incomplete mixing occurs. New stars form out of material which was influenced by several SNe of different masses. Therefore, they do not show the typical abundance pattern of a single SN, but show an average of the SNe which contributed to the enrichment of the local ISM. The spread in the metallicities gradually decreases from [Fe/H] $= -3.0$ to -2.0, reflecting the ongoing mixing process as more and more SNe pollute the ISM. At the beginning of the well-mixed phase, star-formation has consumed about 2.5% of the total halo ISM mass.

This late phase is characterized by a well mixed ISM and begins at [Fe/H] > -2.0, where the abundance scatter in the model is reduced to a third of its initial value. At this stage, the whole volume considered was influenced several times by SN events. This leads to an IMF averaged [El/Fe] ratio in the ISM which is the same as predicted by simple 1-zone models and which is observed in stars with metallicity [Fe/H] > -2.0. Even in an enriched medium, however, a SN event will still have an influence on its neighbourhood, although the change in the abundance pattern will not be as prominent as in a very metal-poor medium. This explains the fact, that even in the well-mixed case, the [El/Fe] ratios show a certain dispersion. At [Fe/H] $= -1.0$, about 8% of the total halo ISM mass has been used to form stars.

The onset of SNe of Type Ia marks the beginning of a third phase in the chemical enrichment history of the galaxy, but we will not consider this phase any further. Note, that the mean [El/Fe] ratios at [Fe/H] $= -1.0$ in our model do not have to be equal to zero (by definition the solar metallicity), since we have neglected the influence of SN Ia events.

To quantify the enrichment of the ISM we introduce the concept of the polluted mass M_{poll} in a unit volume at time τ. It is defined as the total mass which gets polluted by N_{SN} *isolated* SNe, where N_{SN} is the number of SNe in the unit volume that occurred during the elapsed time τ. For a constant mixing-mass M_{sw} swept up by a SN event, $M_{\mathrm{poll}} = N_{\mathrm{SN}} \cdot M_{\mathrm{sw}}$. Since the polluted mass is directly proportional to the number of SNe, it can become larger than the total ISM mass in the unit volume, M_{tot}. Furthermore, the pollution factor f_{poll} is defined as the ratio $M_{\mathrm{poll}}/M_{\mathrm{tot}}$ and only depends on N_{SN}, for fixed M_{sw} and M_{tot}. When $f_{\mathrm{poll}} = 1$, enough SNe have contributed to the chemical enrichment to theoretically pollute the entire ISM in the unit volume, even though there still may be patches of

Table 2. Pollution factor and SN Type II frequency.

[Fe/H]	$f_{\rm poll}$	$N_{\rm SN}$ [kpc^{-3}]	τ [Myr]
-3.5	0.2	27	82
-3.0	0.7	83	170
-2.5	2.1	260	430
-2.0	6.5	810	1430

material which were not yet affected by any SN. A higher pollution factor results in a better mixing of the halo ISM, decreasing the local abundance differences and the amount of material with primordial abundances. Therefore, the ratio $M_{\rm sw}/M_{\rm tot}$ determines the mixing efficiency in our model, i.e. how many SNe in the unit volume are needed to reach a certain value of $f_{\rm poll}$. Given $f_{\rm poll}$, $M_{\rm sw}$ and the mean, IMF integrated iron yield $\langle M_{\rm Fe}\rangle$ of a typical SN II, the mean metallicity of the ISM then is determined by

$$[{\rm Fe/H}] = \log \frac{N_{\rm SN}\cdot\langle M_{\rm Fe}\rangle}{M_{\rm tot}} - C = \log \frac{f_{\rm poll}\cdot\langle M_{\rm Fe}\rangle}{M_{\rm sw}} - C,$$

where C is the solar iron abundance.

The local inhomogeneities of the ISM begin to disappear when most of the gaseous SN remnants start to overlap. This is the case when more or less every cloud in the halo was influenced at least once by a SN event, i.e. the pollution factor is about equal to one. With the adopted mixing mass of $M_{\rm sw} = 5\times10^4\,{\rm M}_\odot$ this is the case at [Fe/H] ≈ -2.8. This metallicity gives an upper limit for the end of the early phase and the beginning of the transition to the second, well-mixed enrichment phase.

Table 2 shows the pollution factor needed to reach the mean metallicities shown in the panels of Fig. 1. Also shown are the corresponding SN frequency $N_{\rm SN}$ and elapsed time τ, which depend on our model parameters. Here, the SN frequency is defined as the number of SNe per kpc^3 and depends on the total ISM mass in the unit volume, whereas the elapsed time scales with the average SFR as

$$\tau' = \tau\cdot\left(\frac{\langle{\rm SFR}\rangle}{1.06\cdot10^{-4}}\right)^{-1},$$

where $1.06\cdot10^{-4}\,{\rm M}_\odot\,{\rm yr}^{-1}\,{\rm kpc}^{-3}$ is the mean SFR in the unit volume in our model. Note that the evolution of the abundance ratios as a function of [Fe/H] is independent of the star formation timescale and the SFR specified in the model.

5.2. Comparison with Observations

The scatter in the [El/Fe] ratios of the model stars as a function of [Fe/H] shows the same general trend for every element considered, independent of the individual stellar yields. The inhomogeneous mixing of the very metal-poor halo ISM at [Fe/H] < -3.0 leads to a scatter in the [El/Fe] ratios of up to 1 dex. This scatter continuously decreases for higher metallicities, reflecting the ongoing mixing of the ISM. At [Fe/H] > -2.0 the model stars show an IMF averaged abundance pattern with an intrinsic scatter of about 0.1 to 0.2 dex. This behaviour matches the general trend of the observations well, as can be seen in Fig. 2. The observations also show a large scatter at low metallicities which again decreases for higher [Fe/H], with some exceptions, however: the iron-group elements Cr and Mn show a strong decrease in the [Cr/Fe] and [Mn/Fe] ratio for lower metallicities. This behaviour can not be reproduced with our adopted metallicity-independent stellar yields and the progenitor-independent mixing mass.

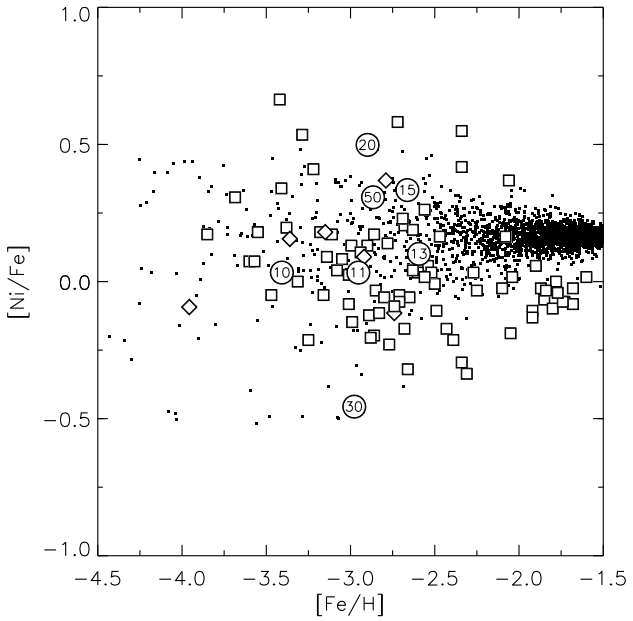

Fig. 3. Normalized nickel-to-iron ratio [Ni/Fe] as function of metallicity [Fe/H]. Symbols are the same as in Fig. 2. The scatter of the model-stars and the halo stars was normalized to unity to highlight the enrichment phases of the halo ISM.

Compared to the observations, the distribution of [Ni/Fe] ratios of the model stars in Fig. 2 shows a scatter that is much too small. This is most likely due to the choice of mass cuts in the SNe II models, which have been set with the aim to reproduce the average solar [Ni/Fe] ratio. Thielemann et al. (1996) discuss in detail that large variations can easily occur. See also the discussion in Sect. 3. We therefore now want to investigate whether the sequence of enrichment stages seen in our model is similar to the observed evolution of abundance ratios even in cases when the employed yields may be incorrect.

To this end we have normalized the scatter in [Ni/Fe] of the model-stars at low [Fe/H] to unity, and have similarly renormalized the range of values for the observed stellar [Ni/Fe] ratios to one. The mean values of both distributions were left unchanged. The resulting renormalized distributions are shown in Fig. 3. The remarkably good agreement of both distributions after this procedure indicates that the enrichment history of the halo ISM implied by the model is consistent with the data, even though the employed Ni yields are not. Based on similar com-

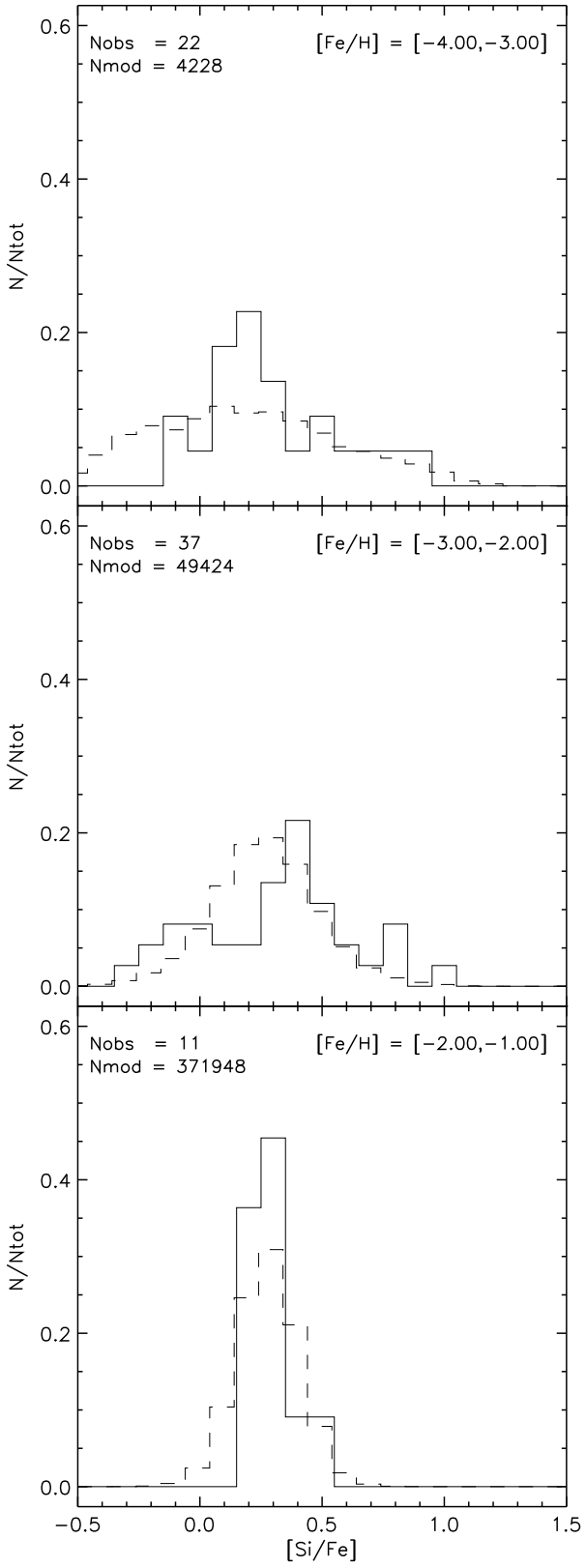

Fig. 4. Relative frequency of stars normalized to unity in [Si/Fe] bins for three different metallicity ranges (see text). The solid line shows observational data, the dashed line the model stars. The number of included stars is given in the upper left corner.

parisons, we conclude that the abundance ratio data of most elements except Mn and Cr are consistent with the predicted enrichment history, and the scatter plots in Fig. 2 can thus be used to compare the range of the theoretically predicted nucleosynthesis yields with observations.

To describe the transition from the metal-poor, unmixed to the enriched, well mixed ISM more quantitatively, the relative frequency of stars at a given [El/Fe] ratio has been analysed for the different enrichment phases. In the case of silicon, this detailed enrichment history is shown in Fig. 4. The different enrichment phases from [Fe/H] < -3.0, $-3.0 <$ [Fe/H] < -2.0 and [Fe/H] > -2.0 are given in the panels from top to bottom. The solid line shows the relative frequency of observed halo stars per [Si/Fe] bin for each enrichment phase and the dashed line the relative frequency of computed model stars per bin. To account for the effect of observational errors on our data, we added a random, normally distributed error with standard deviation 0.1 dex in the [El/Fe] and [Fe/H] ratios to the model stars. The bin size in the [Si/Fe] ratio is 0.1 dex for observed and computed stars, while the position of the histogram for the model stars is shifted by 0.01 dex to the left for better visibility. The total number of stars included in the plot is given in the upper left corner of each panel, where $N_{\rm obs}$ and $N_{\rm mod}$ are the number of observed stars and of model stars, respectively.

In the upper panel, the distributions of both the 22 observed and the 4226 model stars show a spread in the [Si/Fe] ratio of more than one dex. The distribution of the model stars shows two wide, protruding wings and a faint peak at [Si/Fe] ≈ 0.2. The "right" wing shows a shallow rise from [Si/Fe] ≈ 1.1 to the peak. The "left" wing is not as extended and shows a rather steep cutoff at [Si/Fe] ≈ -0.3. This asymmetry is due to the nucleosynthesis models of core-collapse SNe, which show a more or less constant value of [Si/Fe] ≈ -0.3 for progenitor masses in the range of $10 - 13\,{\rm M}_{\odot}$, as can be seen in Fig. 2. The distribution of the halo stars peaks at the same location as the model stars but extends only down to [Si/Fe] ≈ -0.1. We attribute this to the poor statistic of the data set, since this gap is filled in the middle panel.

The middle panel of Fig. 4 shows the same distribution for the intermediate mixing stage of the ISM. The distribution of the model stars now has smaller wings, and peaks at [Si/Fe] ≈ 0.3. It is still broader than 1 dex, but the majority of the stars fall near the IMF averaged [Si/Fe] ratio. The prominent peak is caused by the already well-mixed regions, whereas the broad distribution shows that the halo ISM is still chemically inhomogeneous. The peak of the observational sample has shifted by about 0.2 dex to the right and lies now at [Si/Fe] ≈ 0.4. Compared to the prediction of the model, the relative frequency of the halo stars is too high in the wings of the distribution and too low to the left of the peak.

The lower panel shows the late stage, where the halo ISM is well mixed. The broad wings have completely disappeared and only the very prominent peak at the IMF averaged value remains. The distributions of the 11 observed stars and the 370 000 model stars are in good agreement. At this metallic-

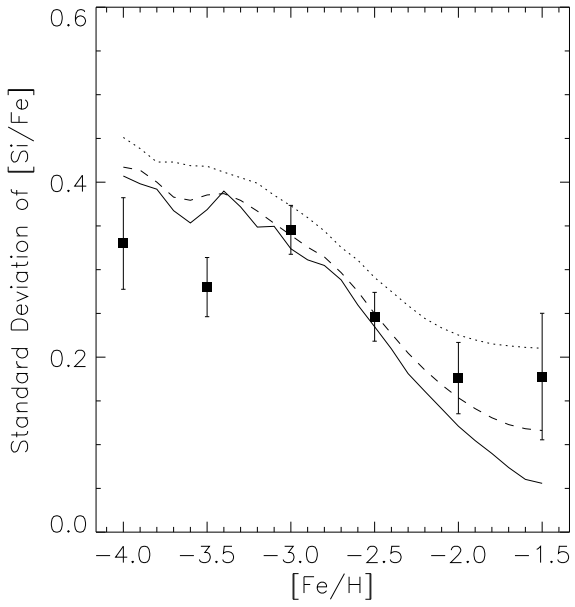

Fig. 5. Scatter in [Si/Fe] of the model and observed stars. The solid line gives the scatter of the model stars, the dashed and dotted lines show the scatter of the model stars, folded with an error of 0.1 and 0.2 dex. Filled squares give the standard deviation of the observed stars (see text).

ity no SN of Type Ia should have polluted the by now well mixed ISM and the metal abundance is high enough to restrict the impact of single SN II events on the ISM.

The most prominent feature which characterizes the different enrichment phases, is the intrinsic scatter in the abundances of metal-poor stars. This can be seen in Fig. 5, which shows the standard deviation of [Si/Fe] as a function of metallicity [Fe/H] for the model and the halo stars. The bin size used to compute the standard deviation was 0.1 dex in metallicity. The solid line shows the scatter of the unmodified model stars. The influence of observational errors on our data was simulated by adding a random, normally distributed error with standard deviation 0.1 and 0.2 dex in both [Si/Fe] and [Fe/H]. The resulting scatter in dependence of metallicity is given by the dashed and dotted lines. In the range of $-4.0 <$ [Fe/H] < -3.0 the scatter has a more or less constant value of approximately 0.4 dex. It declines rather steeply in the range $-3.0 <$ [Fe/H] < -2.0 and levels off again at metallicities higher than -2.0, depending on the assumed observational errors of 0.0, 0.1 or 0.2 dex. These curves show that for errors in this range the scatter at low metallicities is dominated by the intrinsic differences in the element abundances of single stars.

For comparison, the scatter in the [Si/Fe] ratio of observed halo stars is represented by filled squares. The observations were binned with a bin size of 0.5 dex to compute the standard deviations. To estimate the reliability of their scatter in [Si/Fe], we built several new data sets by adding a normally distributed random error with standard deviation 0.1 dex to the [Si/Fe] ratio and the metallicity of the stars. For each new data set, the standard deviation in the different bins was computed. The standard deviation for the results from these artificial data sets is given in the plot as 1-σ error-bars. The scatter of the observed abundance ratios shows nicely the features already seen in the curves for the model stars. At the first stage of the enrichment, it is approximately constant, followed by a steady decline in the intermediate mixing phase. At higher metallicities, the scatter levels off again.

Since the scatter in [Si/Fe] at [Fe/H] $= -4.0$ is about 0.4 dex the observational errors have little influence on the analysis at these low metallicities, unless unknown systematic or confusion errors were large enough to inflate the scatter at [Fe/H] $= -4.0$ to also about 0.4 dex. On the other hand, observational errors do dominate the scatter at metallicities [Fe/H] > -2.0, when the halo ISM is well mixed and the intrinsic scatter of the stars is negligible compared to the observational errors.

5.3. Individual Elements and Nucleosynthesis

Oxygen & Magnesium: As expected, the IMF averaged [El/Fe] ratios for O and Mg reproduce the mean abundance of the observed metal-poor stars nicely. The [O/Fe] ratio seems to be slightly too low, whereas [Mg/Fe] is slightly too high, but both deviations are smaller than 0.1 dex. No trend in the observational data of Mg can be seen and a trend in O only becomes visible if the observations of Israelian et al. (1998) are considered.

An important fact is that the scatter in the data, although increasing at lower metallicities, does not match the large scatter of more than two dex predicted by the stellar yields. Since no other mixing effects than the overlapping of SN remnants are included in our model, the expected scatter is determined by the nucleosynthesis yields. If gas flows and the random motion of stars in the halo accelerated the chemical mixing, a smaller scatter in the model data would be expected. Even then, the fact that the observed stars only show [O/Fe] or [Mg/Fe] ratios corresponding to the stellar yields produced by $18 - 50\,\mathrm{M}_{\odot}$ SNe would remain unexplained.

If we assume a top-heavy IMF which favoured high-mass SNe, this problem could be solved. However, the abundance pattern of the other elements should then also reflect this, which is not the case. This leaves us with two explanations: Either the stellar yields of O *and* Mg or of Fe are incorrect (or both).

Since the exact location of the mass cut is not known, the actual Fe yields are not very well determined (Woosley & Weaver 1995; Thielemann et al. 1996) and direct observational information which links a progenitor to an ejected Fe mass is very limited, maybe with the exception of SN 1987A and 1993J. Otherwise only the IMF integrated Fe-yields are constrained, but not necessarily their progenitor mass dependence (declining, rising, or with a maximum, see Nakamura et al. 1999 and Sect. 3). In order to attain a fit to the observational data within our evolution model we would need to decrease the Fe yields of the 13 or $15\,\mathrm{M}_{\odot}$ stars by a factor of six. Without

adjusting Fe-yields of the more massive stars, and assuming a standard Salpeter IMF, this would increase the IMF averaged [O/Fe] and [Mg/Fe] ratio by about 0.3 dex (a factor of two) and would therefore result in a much too high IMF averaged value. Equally, every other abundance ratio would be affected by this change.

On the other hand, the stellar yields of the α-elements O and Mg could be too low for the 13 and $15\,\mathrm{M}_{\odot}$ progenitors. The abundances of O and Mg are mainly determined in the hydrostatic burning phases and do not depend heavily on the explosion mechanism. Changing the stellar yields of O and Mg for the 13 and $15\,\mathrm{M}_{\odot}$ progenitor stars would therefore require to adjust the existing stellar models, which suffer from uncertainties in the theory of convection and the treatment of rotation.

Silicon: The IMF averaged [Si/Fe] ratio and the scatter predicted by the stellar yields fit the observations perfectly. The decrease in the scatter for higher metallicities and therefore the different enrichment phases of the halo ISM are clearly visible. At [Fe/H] < -3.0, the scatter in the model points reflects the scatter predicted by the stellar yields. During the transition from the unmixed to the well mixed ISM, in the range $-3.0 <$ [Fe/H] < -2.0, the scatter decreases steadily and leads to the IMF averaged [Si/Fe] ratio, which is reached at [Fe/H] > -2.0.

Calcium: The IMF averaged [Ca/Fe] ratio is about 0.2 dex lower than the observed mean for metal-poor stars. If the model data is shifted by this value to reproduce the mean of the observational data, the scatter for very metal-poor stars and the transition to the less metal-poor stars fits the data well. Note that, contrary to the other α-elements, the stellar yields of Ca are no longer approximately proportional to the mass of the progenitor. This behaviour becomes more pronounced in the cases of Cr, Mn and Ni.

Chromium & Manganese: The iron-peak elements Cr and Mn are both produced mainly during explosive silicon burning and show an almost identical, complicated dependence on the mass of the progenitor. The IMF averaged [El/Fe] ratio reproduces the observations of the less metal-poor stars well. The scatter predicted by the stellar yields is only about 0.8 dex and is not as large as for the α-elements.

A notable feature of the observations is the decrease of the [Cr/Fe] and [Mn/Fe] ratios for lower metallicities, seen in the newer data. If these trends are real, they can not be reproduced by metallicity-independent yields unless one assumes a progenitor mass dependent amount of mixing with the interstellar medium (Nakamura et al. 1999).

The upper limits of the [El/Fe] ratios of Cr and Mn are given by the stellar yields of a $30\,\mathrm{M}_{\odot}$ SN and correspond to the highest [Cr/Fe] and [Mn/Fe] ratios seen in metal-poor stars, with the exception of the binary CS 22876-032 which shows an unusual high [Mn/Fe] ratio of 0.29 dex. Recent high-signal-to-noise, high-resolution data result in a lower [Mn/Fe] value for this star, placing it near the IMF averaged value (S. G. Ryan, private communication). On the other hand, the lower limits of the observed [Cr/Fe] and [Mn/Fe] ratios do not correspond at all with those given by the stellar yields, which show a ratio

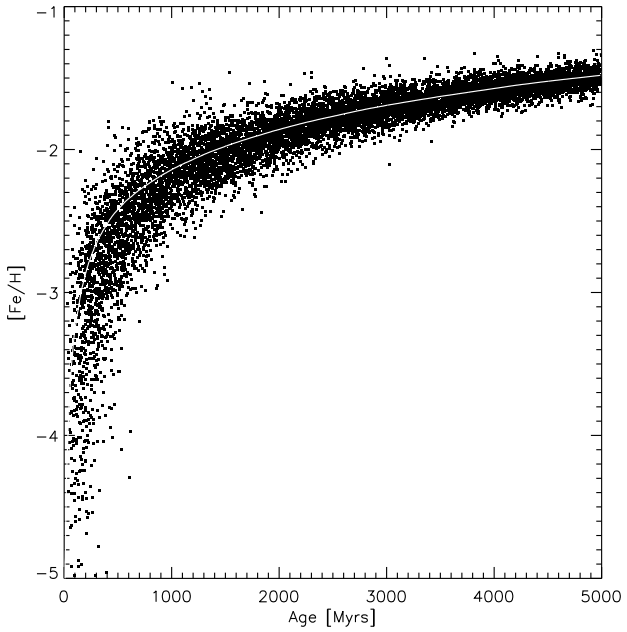

Fig. 6. Metallicity [Fe/H] vs. age of single model stars.

which is too high by up to 0.5 dex in the Thielemann et al. (1996) yields. Only a different choice of mass cuts as a function of progenitor mass (Nakamura et al. 1999) or as a function of metallicity would be able to rectify this.

Nickel: The stellar yields of the most important iron-peak element besides Fe completely fail to reproduce the observations. The scatter of the stellar yields is only about 0.5 dex compared to about 1.2 dex seen in the observational data. Compared to the mean of the observations, the IMF averaged abundance of the model-stars is about 0.1 dex to high. The small scatter in the [Ni/Fe] ratio originates from an almost constant ratio of Ni and Fe yields, which means that in the models Ni is produced more or less proportional to iron. To reproduce the scatter seen in the observations, Ni would have to depend on the progenitor mass differently from Fe. This is a shortfall of the employed yields, adjusted to reproduce the average solar [Ni/Fe] ratio with the choice of their mass cuts. Varying neutron excess in the yields, however, can change the [Ni/Fe] ratio drastically (Thielemann et al. 1996 and Sect. 3).

Europium: The r-process element Eu reproduces the scatter and the mean of the observational data quite well. But compared to the α-elements O, Mg, Si and Ca its behaviour is very different. The highest [Eu/Fe] ratio is produced by low mass SN and the lowest ratio by high mass SN, as required when one constructs yields under the assumption that the r-process originated from SNe II (see Sect. 3). This is exactly the opposite to what is found for the α-elements. Therefore, a top-heavy IMF would lead to a steadily increasing [Eu/Fe] ratio, since the most massive SNe will explode first (cf. *Oxygen & Magnesium*).

5.4. Age–Metallicity Relation

Common 1-zone chemical evolution models are based on the assumption that the system is well mixed at all times. An important consequence of this assumption is a monotonically increasing metallicity, which leads to a well defined age–metallicity relation. Therefore, it is in principle possible to deduce the age of a star if its metallicity is known. This basic assumption of 1-zone chemical evolution models was dropped in our stochastic approach. Therefore, it is not surprising that the well defined age–metallicity relation has to be replaced by a statistical relation. In Fig. 6, the metallicity [Fe/H] of model stars is plotted against the time of their formation. Model stars are represented by small filled squares. For comparison the white line visible in the middle of the black strip shows the mean age–metallicity relation, corresponding to the relation given by a 1-zone model. As can be seen, there is no clear age–metallicity relation at any time. Stars which were formed in the first 500 million years show a metallicity ranging from [Fe/H] < -4.0 up to [Fe/H] > -2.0 and in one extreme case up to [Fe/H] ≈ -1.5. On the other hand, stars with metallicity [Fe/H] $= -2.0$ could have formed at any time in the first 3×10^9 years. Taking these huge uncertainties into account, it is no longer possible to speak of a well-defined age–metallicity relation.

While the mean [Fe/H] abundance increases about linearly with time, the scatter in Fig. 6 again reflects the different enrichment phases of the ISM. The steep rise at early times marks the metal-poor and chemically inhomogeneous stage of the halo ISM. Contrary to this first phase, where SN events dominated the metal-poor ISM locally and the enrichment of isolated clouds could be very efficient, the late stage is characterized by a well mixed ISM and therefore an inefficient enrichment, which is reflected by the slow increase of the age–metallicity "relation" at later times.

5.5. Ultra Metal-poor Stars

From our calculations, we can deduce the number of metal-poor stars which we expect to observe in different metallicity bins. The normalized distribution is shown in Fig. 7 for bin sizes of 0.2 dex and 1.0 dex. The number distribution is approximately a power law with slope 0.7 for [Fe/H] < -3.5 and slope 0.9 for [Fe/H] > -3.0. Also plotted are the observed data from a homogeneous intermediate resolution sample of Ryan & Norris (1991) and the combined high resolution data from Table 1, both rebinned to the large bin size (see Tables 3 and 4 for the numerical values). It is possible that the high resolution sample is incomplete in the range $[-3.0, -2.0]$, whereas the intermediate resolution sample might have a shortage of stars with [Fe/H] < -3.0. Table 3 also lists the number of model stars expected in the three 1.0 dex bins, normalized such that the number of model stars in the range $-4.0 <$ [Fe/H] < -3.0 is equal to the number of observed halo stars in the high-resolution sample in this metallicity range. As can be seen, in this case we expect 5 ± 2 model stars with $-5.0 <$ [Fe/H] < -4.0 while the high resolution sample contains none. If the ratio of stars in these two metallicity bins for this admittedly inhomogeneous sample is representative for the Galactic halo stars, this would suggest a genuine shortage of the most metal-poor stars. In this case a possible solution could be the pre-enrichment of the halo ISM by population III stars. It is conceivable that these already produced an iron abundance of [Fe/H] ≈ -4.0 before they disappeared, leaving only a pre-enriched ISM.

Table 3. Top: Relative frequency of stars in the homogeneous intermediate resolution survey of Ryan & Norris (1991), the combined high resolution data from Table 1 and our model, binned with binsize 1 dex.
Bottom: Absolute numbers. The last row gives the number of stars per bin which we expect to be present, if our model gives a fair representation of the halo metallicity distribution. The number of model-stars is normalized to the number of stars in the range $-4.0 <$ [Fe/H] < -3.0 in the high resolution sample. No star was detected with confirmed [Fe/H] < -4.0, in contrast to the 5 ± 2 stars predicted by the model.

[Fe/H]	$[-3.0, -2.0]$	$[-4.0, -3.0]$	$[-5.0, -4.0]$
Ryan & Norris	0.943	0.057	0.000
High resolution	0.654	0.346	0.000
Model	0.865	0.115	0.020
Ryan & Norris	99	6	0
High resolution	53	28	0
Expected	211 ± 15	28 ± 5	5 ± 2

Table 4. Relative frequency of model stars, binned with binsize 0.2 dex.

[Fe/H]	N/N_{tot}	$\log(N/N_{tot})$
$[-5.0, -4.8]$	$1.92 \cdot 10^{-03}$	-2.72
$[-4.8, -4.6]$	$2.37 \cdot 10^{-03}$	-2.63
$[-4.6, -4.4]$	$3.43 \cdot 10^{-03}$	-2.46
$[-4.4, -4.2]$	$5.10 \cdot 10^{-03}$	-2.29
$[-4.2, -4.0]$	$7.51 \cdot 10^{-03}$	-2.12
$[-4.0, -3.8]$	$1.00 \cdot 10^{-02}$	-2.00
$[-3.8, -3.6]$	$1.31 \cdot 10^{-02}$	-1.88
$[-3.6, -3.4]$	$1.93 \cdot 10^{-02}$	-1.71
$[-3.4, -3.2]$	$2.82 \cdot 10^{-02}$	-1.55
$[-3.2, -3.0]$	$4.41 \cdot 10^{-02}$	-1.36
$[-3.0, -2.8]$	$6.71 \cdot 10^{-02}$	-1.17
$[-2.8, -2.6]$	$1.02 \cdot 10^{-01}$	-0.99
$[-2.6, -2.4]$	$1.47 \cdot 10^{-01}$	-0.83
$[-2.4, -2.2]$	$2.11 \cdot 10^{-01}$	-0.68
$[-2.2, -2.0]$	$3.38 \cdot 10^{-01}$	-0.47

6. Conclusions & Discussion

We have developed a stochastic model of the early chemical enrichment of the halo ISM. The aim of the model is to understand the scatter in the [El/Fe] ratios of observed stars at

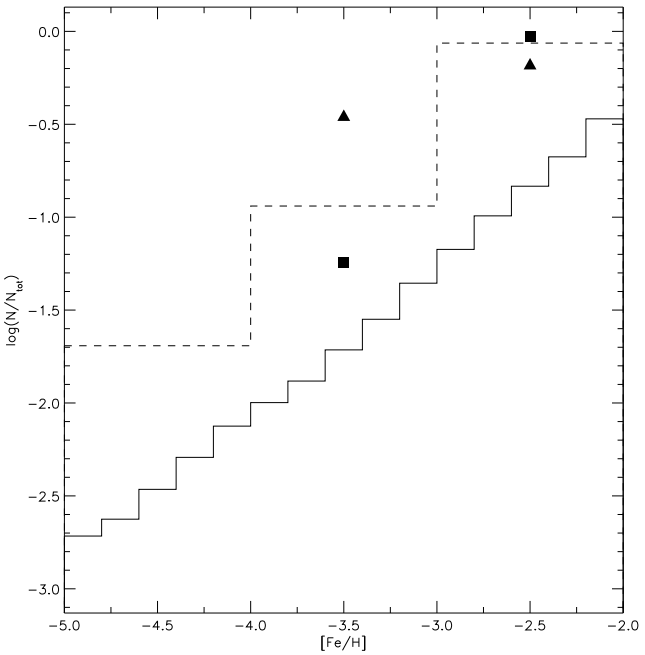

Fig. 7. Metallicity distribution in the model at the end of the calculation ([Fe/H]$= -1$). The number of stars with metallicity [Fe/H] is shown (a) in bins of 0.2 dex (b) in bins of 1.0 dex. In both cases the total number of stars is normalized to one. The solid squares show the intermediate resolution data of Ryan & Norris (1991), the solid triangles the combined high resolution data from Table 1, both binned with bin size 1.0 dex and similarly normalized. There are no observed stars with [Fe/H] < -4.0. See Tables 3, 4 and text.

very low metallicities and the transition to the smaller scatter seen at higher metallicities. We computed the evolution of the abundances of the α-elements O, Mg, Si and Ca, the iron-peak elements Cr, Mn, Fe and Ni and the r-process element Eu and investigated the mixing of the halo ISM.

We divide the enrichment history of the halo ISM into different phases. At metallicities [Fe/H] < -3.0, the ISM is not mixed and is dominated by local abundance inhomogeneities, which are caused by individual Type II SNe of different progenitor masses. The second phase at [Fe/H] > -2.0 is defined by a well mixed ISM which shows IMF averaged abundances and is too metal-rich to be dominated by single SN events. A continuous transition from the first to the second phase occurs between $-3.0 <$ [Fe/H] < -2.0. The onset of SN Ia events marks the beginning of a third phase in the enrichment of the ISM.

The different enrichment phases of the halo ISM can be distinguished in every considered element, after normalising to the stellar yields. On the other hand, Fig. 2 shows that some stellar yields reproduce the IMF averaged element-to-iron ratio [El/Fe] well, but fail to reproduce the abundance scatter observed in metal-poor halo stars. Especially the stellar yields of the α-elements O and Mg predict stars with a low element-to-iron ratio ([O/Fe] or [Mg/Fe] < 0.0), which are not observed. Typically, metal-poor halo stars show an overabundance of α-elements of about [α/Fe] ≈ 0.3 to 0.4, as can be seen in Fig. 2. This is especially troublesome, since an attempt to solve this problem would either require a change in the iron yields of the 13 and 15 $M_\odot$ models of up to a factor six, which would raise every other mean element abundance by about 0.3 dex (a factor of two), or a change in the stellar yields of oxygen and magnesium, which are produced mainly during the hydrostatic burning phases.

Recent observations of metal-poor stars show a decrease of the [Cr/Fe] and [Mn/Fe] ratios for lower metallicities. It is not possible to explain these trends with the metallicity independent stellar yields we have used. Also, the stellar yields of the iron-peak element Ni predict a scatter in [Ni/Fe] which is much too small compared to the observational data. These problems argue strongly for a revision of the theoretical nucleosynthesis models and their extension to lower metallicities.

The unfortunate situation is, however, that there exists no theoretical foundation to do so for Fe-group yields as long as the supernova explosion mechanism is not understood. Thielemann et al. (1996) discussed in detail uncertainties of Fe-group yields due to the choice of mass cut, explosion energy and entropy, as well as the delay time between collapse and explosion, affecting also the neutron-richness of matter. Multidimensional aspects might add further degrees of freedom (Nagataki et al. 1997, 1998). Thus, there is an understanding of dependences, coincidences of abundance features etc., but at present only observational information combined with galactic evolution modelling like in the present paper or, e.g., Tsujimoto & Shigeyama (1998) and Nakamura et al. (1999) can try to provide sufficient constraints for a further understanding of supernova nucleosynthesis.

The advancing enrichment process of the halo ISM can be characterized by the pollution factor $f_{\rm poll}$, defined as the ratio of the mass $M_{\rm poll} = N_{\rm SN} \cdot M_{\rm sw}$ polluted by $N_{\rm SN}$ preceding SNe and the ISM mass $M_{\rm tot}$, all in a unit volume. The enrichment history of the halo ISM now is mainly determined by the mixing efficiency which in turn is fixed by the ratio of the mass $M_{\rm sw}$ of swept-up material in a SN event and $M_{\rm tot}$. The more mass a SN sweeps up, the less SN events are needed to reach a certain value of $f_{\rm poll}$, making the mixing more efficient. $M_{\rm sw}$ also determines the average metallicity [Fe/H] of the halo ISM for a given pollution factor. A larger swept-up mass leads to a lower mean ISM metallicity and vice versa. Therefore, the metallicity where the transition from one enrichment stage to the next occurs, depends only on the mixing efficiency $M_{\rm sw}/M_{\rm tot}$ and not on the SFR. The SFR is only important if one is interested in the *elapsed time* that is needed to reach a certain mean metallicity of the halo ISM.

Figures 4 and 5 support our adopted value of $5 \times 10^4\,M_\odot$ of swept up material. If the swept up mass is higher, the mixing would be more efficient, resulting in an IMF averaged chemical abundance pattern at lower metallicities. This would produce a narrower peak in Fig. 4 and a steeper slope in Fig. 5. Moreover, the whole curve in Fig. 5 would be shifted towards lower

metallicities. On the other hand, a smaller mixing mass would reduce the efficiency of the enrichment of the ISM, which could be seen in a broader distribution at higher metallicities in Fig. 4 and a shallower slope in Fig. 5.

Standard 1-zone chemical evolution models predict a well defined age–metallicity relation, based on the assumption that the ISM is well mixed at all times. In our stochastic model the chemical inhomogeneity of the halo ISM and therefore the scatter in metallicity at any time is much too high to reasonably establish such a relation. Nevertheless, the steep rise with large scatter seen in Fig. 6 at very early times marks the chemically inhomogeneous enrichment phase, while the slow increase later-on reflects the well mixed, metal-rich ISM.

The results of our model also quantify the problem of the missing ultra metal-poor stars. From it we have deduced the expected number of ultra metal-poor stars (with [Fe/H] < -4.0) which should have been observed, normalized to the number of halo stars in the combined high-resolution sample with metallicities in the range $-4.0 <$ [Fe/H] < -3.0. We expect about 5 ± 2 ultra metal-poor stars whereas none was found to date. It is possible that Population III stars have caused a pre-enrichment of the ISM to [Fe/H] ≈ -4.0 and already have disappeared before the onset of the formation of the Galaxy.

We would like to thank the referee S. G. Ryan for helpful and motivating discussions and for providing us with some of the observational data. This work was supported by the Swiss Nationalfonds.

References

Balachandran, S. C., Carney, B. W., 1996, AJ, 111, 946
Bessel, M. S., Sutherland R. S., Ruan K., 1991, ApJ, 383, L71
Beveridge, R. C., Sneden, C., 1994, AJ, 108, 285
Binney, J., Tremaine, S., 1987, Galactic Dynamics, Princeton University Press, Princeton, New Jersey
Boesgaard, A. M., King, J. R., Deliyannis, C. P., Vogt, S. S., 1999, AJ, 117, 492
Bouchet, P., Danziger, I. J., Lucy, L. B., 1991, AJ, 102, 1135
Buchmann, L., 1996, ApJ, 468, L127
Buchmann, L., 1997, ApJ, 479, L153
Burrows, A., 1990, Ann. Rev. Nucl. Part. Sci., 40, 181
Burrows, A., Hayes, J., Fryxell, B., 1995, ApJ, 450, 830
Burrows, A., 1996, Nucl. Phys., A606, 151
Burrows, A., Sawyer R. F., 1998, Phys. Rev., C58, 554
Charbonnel, C., Meynet, G., Maeder, A., Schaller, G., Schaerer, D., 1993, A&AS, 101, 415
Carney, B. W., Laird, J. B., Latham, D. W., Aguilar, L. A., 1996, AJ, 112, 668
Chiappini, C., Matteucci, F., Beers, T. C., Nomoto, K., 1999, ApJ, 515, 226
Chiba, M., Yoshii, Y., 1998, AJ, 115, 168
Chieffi, A., Limongi, M., Straniero, O., 1998, ApJ, 502, 737
Cioffi, D. F., McKee, C. F., Bertschinger, E., 1988, ApJ, 334 252
Cowan, J. J., Sneden, C., Ivans, I., Burles, S., Beers, T. C., Fuller, G., 1999, BAAS, 194, 67.04
François, P., Spite, M., Spite, F., 1993, A&A, 274, 821
Freiburghaus, C., Rembges, F., Rauscher, T., Kolbe, E., Thielemann, F.-K., Kratz, K.-L., Pfeiffer, B., Cowan, C., 1999, ApJ, 516, 381
Freiburghaus, C., Rosswog, S., Thielemann, F.-K., 1999, ApJ 525, L121
Fuhrmann, K., Axer, M., Gehren, T., 1995, A&A, 301, 492
Gratton, R. G., 1989, A&A, 208, 171
Gratton, R. G., Sneden, C., 1991a A&A, 241, 501
Gratton, R. G., Sneden, C., 1991b A&A, 287, 927
Harris, W. E., Bell, R. A., Vandenberg, D. A., Bolte, M., Stetson, P. B., Hesser, J. E., Van Den Bergh, S., Bond, H. E., Fahlman, G. G., Richer, H. B., 1997, AJ, 114, 1030
Heger, A., Langer, N., Woosley, S. E., 1999, ApJ, astro-ph/9904132 (in press)
Henry, R. B. C., 1984, ApJ, 281, 644
Herant, M., Benz, W., Hix, W. R., Fryer, C. L., Colgate, S. A., 1994, ApJ, 435, 339
Hoffman, R. D., Woosley, S. E., Weaver, T. A., Rauscher, T., Thielemann, F.-K., 1999, ApJ, 521, 735
Ishimaru, Y., Wanajo, S., 1999, ApJ, 511, L33
Israelian, G., Garcia, L., Ramón, J., Rebolo, R., 1998, ApJ, 507, 805
Iwamoto, K., Nomoto, K., Höflich, P., Yamaoka, H., Kumagai, S., Shigeyama, T., 1994, ApJ 437, L115
Iwamoto, K., Mazzali, P. A., Nomoto, K., Umeda, H., Nakamura, T., Patat, F., Danziger, I. J., Young, T. R., Suzuki, T., Shigeyama, T., Augusteijn, T., Doublier, V., Gonzalez, J.-F., Boehnhardt, H., Brewer, J., Hainaut, O. R., Lidman, C., Leibundgut, B., Cappellaro, E., Turatto, M., Galama, T. J., Vreeswijk, P. M., Kouveliotou, C., Van Paradijs, J., Pian, E., Palazzi, E., Frontera, F., 1998, Nature 395, 672
Iwamoto, K., 1999, ApJ, 512, L67
Iwamoto, K., 1999, ApJ, 517, L47
Janka, H.-T., Müller, E., 1995, Phys. Rep., 256, 135
Janka, H.-T., Müller, E., 1996, A&A, 306, 167
Jehin, E., Magain, P., Neuforge, C., Noels, A., Parmentier, G., Thoul, A. A., 1999, A&A, 341, 241
Keil, W., Janka, H.-T., 1995, A&A, 296, 145
Kozma, C., Fransson, C., 1998, ApJ, 497, 431
King, J. R., 1994, ApJ, 436, 331
Langer, N., Henkel, C., 1995. In: Busso, M., Gallino, R., Raiteri, C. M. (eds.) Nuclei in the Cosmos III. AIP Press, p.413
Langer, N., Fliegner, J., Heger, A., Woosley, S. E., 1997, Nucl. Phys., A621, 457c
Larson, R. B., 1988. In: R. E. Pudritz, M. Fich (eds.) Galactic and Extragalactic Star Formation. NATO ASI Series 232, 5, Kluwer, Dordrecht
Magain, P., 1989, A&A, 209, 211
Mathews, G. J., Bazan, G., Cowan, J. J., 1992, ApJ, 391, 719
Matteucci, F., Romano, D., Molaro, P., 1999, A&A, 341, 458
McWilliam, A., Preston, G. W., Sneden, C., Searle, L., 1995, AJ, 109, 2757
McWilliam, A., 1997, ARA&A, 35, 503
Messer, O. E. B., Mezzacappa, A., Bruenn, S. W., Guidry, M. W., 1998, ApJ, 507, 353
Meynet, G., Maeder, A., 1997, A&A, 321, 465
Mezzacappa, A., Calder, A. C., Bruenn, S. W., Blondin, N. J. M., Guidry, M. W., Strayer, M. R., Umar, A. S., 1998, ApJ, 495, 911
Molaro, P., Bonifacio, P., 1990, A&A, 236, L5
Molaro, P., Castelli, F., 1990, A&A, 228, 426
Nakamura, T., Umeda, H., Nomoto, K., Thielemann, F.-K.,, Burrows, A., 1999, ApJ, 517, 193
Nagataki, S., Hashimoto, M., Sato, K., Yamada, S., 1997, ApJ, 486, 1026
Nagataki, S., Hashimoto, M., Sato, K., Yamada, S., Mochizuki, Y. S., 1998, ApJ, 492, L45

Nissen, P. E., Gustafsson, B., Edvardsson, B., Gilmore, G., 1994, A&A, 285, 440
Nomoto, K., Hashimoto, M., 1988, Phys. Rep., 163,
Nomoto, K., Hashimoto, M., Tsujimoto, T., Thielemann, F.-K., Kishimoto, N., Kubo, Y., Nakasato, N., 1997, Nucl. Phys., A161, 79c13
Norris, J. E., Peterson, R. C., Beers, T. C., 1993, ApJ, 415, 797
Peterson, R. C., Kurucz, R. L., Carney, B. W., 1990, ApJ, 350, 173
Pons, J. A., Reddy, S., Prakash, M., Lattimer, J. M., Miralles, J. A., 1999, ApJ, 513, 780
Primas, F., Molaro, P., Castelli, F., 1994, A&A, 290, 885
Reddy, S., Prakash, M., 1997, ApJ, 423, 689
Ryan, S. G., Norris, J. E., Bessell, M. S., 1991, AJ, 102, 303
Ryan, S. G., Norris, J. E., 1991, AJ, 101, 1865
Ryan, S. G., Norris, J. E., Beers, T. C., 1996, ApJ, 471, 254
Saio, H., Nomoto, K., ApJ, 500, 388
Samland, M., 1997, ApJ, 496, 155
Schaerer, D., Meynet, G., Maeder, A., Schaller, G., 1993, A&AS, 98, 523
Schaerer, D., Charbonnel, C., Meynet, G., Maeder, A., Schaller, G., 1993, A&AS, 102, 339
Schaller, G., Schaerer, D., Meynet, G., Maeder, A., 1992, A&AS, 96, 269
Shigeyama, T., Nomoto, K., 1990, ApJ, 360, 242
Shigeyama, T., Tsujimoto, T., 1998, ApJ, 507, L 135
Sneden, C., Preston, G. W., McWilliam, A., Searle, L., 1994, ApJ, 431, L27
Sollerman, J., Leibundgut, B., Spyromilio, J., 1998, A&A, 337, 207
Spruit, H. C., 1992, A&A, 253, 131
Spiesman, W. J., Wallerstein, G., 1991, AJ, 102, 1790
Spite, M., Spite, F., 1991, A&A, 252, 689
Suntzeff, N. B., Phillips, M. M., Elias, J. H., Walker, A. R., Depoy, D. L., 1992, ApJ, 384, L33
Takahashi, K., Witti, J., Janka, H.-T., 1994, A&A, 286, 857
Talon, S., Zahn, J.-P., Maeder, A., Meynet, G., 1997, A&A, 322, 209
Thielemann, F.-K., Nomoto, K., Hashimoto, M., 1996, ApJ, 460, 408
Thomas, D., Greggio, L., Bender, R., 1998, MNRAS, 296, 119
Travaglio, C., Galli, D., Gallino, R., Busso, M., Ferrini, F, Staniero, O., 1999, ApJ, 521, 691
Tsujimoto, T., Shigeyama, T., 1998, ApJ, 508, L151
Turatto, M., Mazzali, P. A., Young, T. R., Nomoto, K., Iwamoto, K., Benetti, S., Cappallaro, E., Danziger, I. J., De Mello, D. F., Phillips, M. M., Suntzeff, N. B., Clocchiatti, A., Piemonte, A., Leibundgut, B., Covarrubias, R., Maza, J., Sollerman, J., 1998, ApJ 498, L129
Umeda et al., 1999, in *First Stars*, ESO (in press)
Wasserburg, G., Busso, M., Gallino, R., 1996, ApJ, 466, L109
Wheeler, J. C., Cowan, J. J., Hillebrandt, W., 1998, ApJ 493, L101
Woosley, S. E., Wilson, J. R., Mathews, G. J., Hoffman, R. D., Meyer, B. S., 1994, ApJ, 433, 229
Woosley, S. E., Weaver, T. A., 1995, ApJS, 101, 181
Yamada, S., Janka, H.-T., Suzuki, H., 1999, A&A, 344, 533
Zhao, G., Magain, P., 1990, A&A, 238, 242

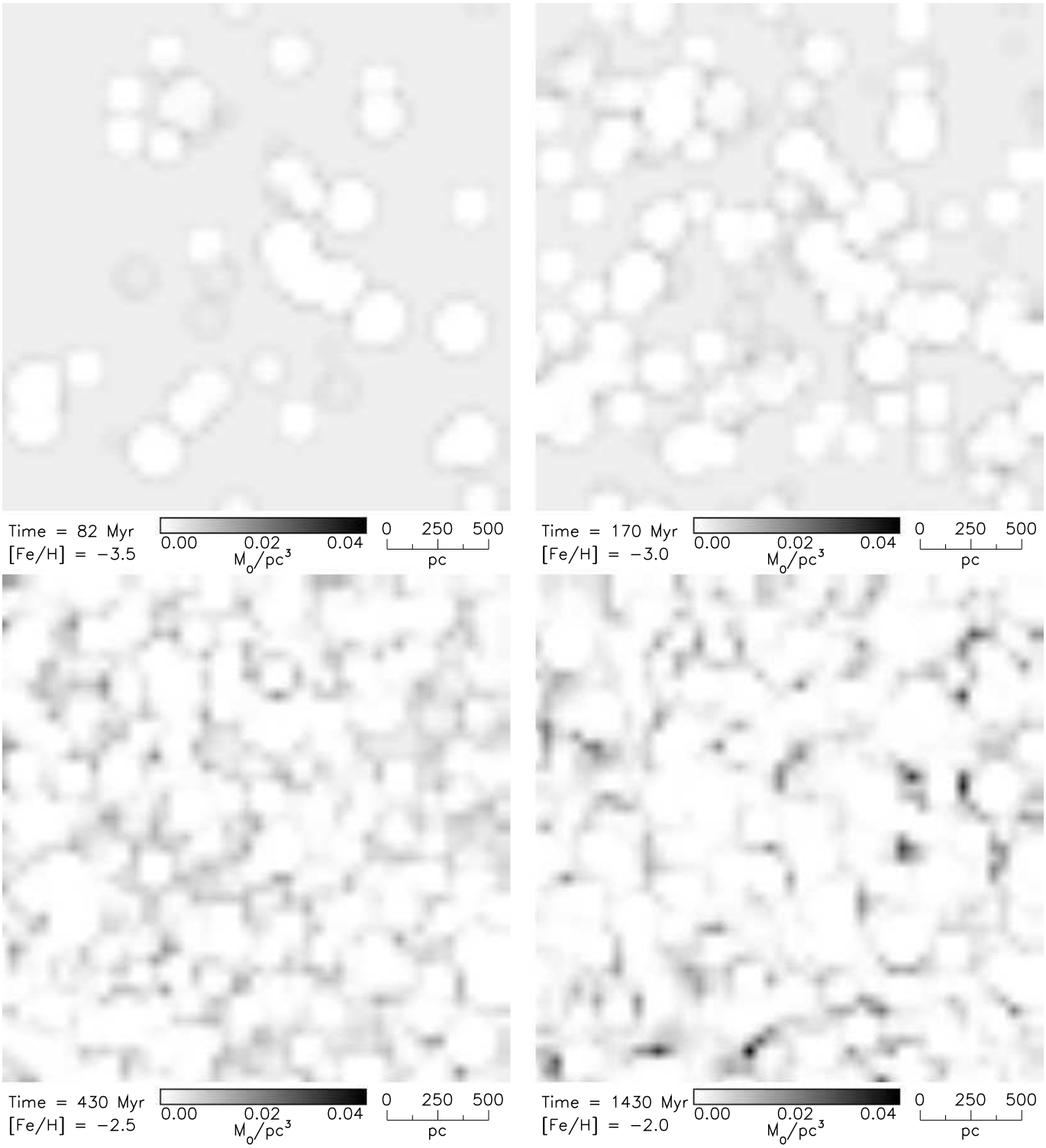

Fig. 1. Cut through the computed volume, showing the density distribution of the halo ISM during the transition from the unmixed to the well mixed stage (see text for details).

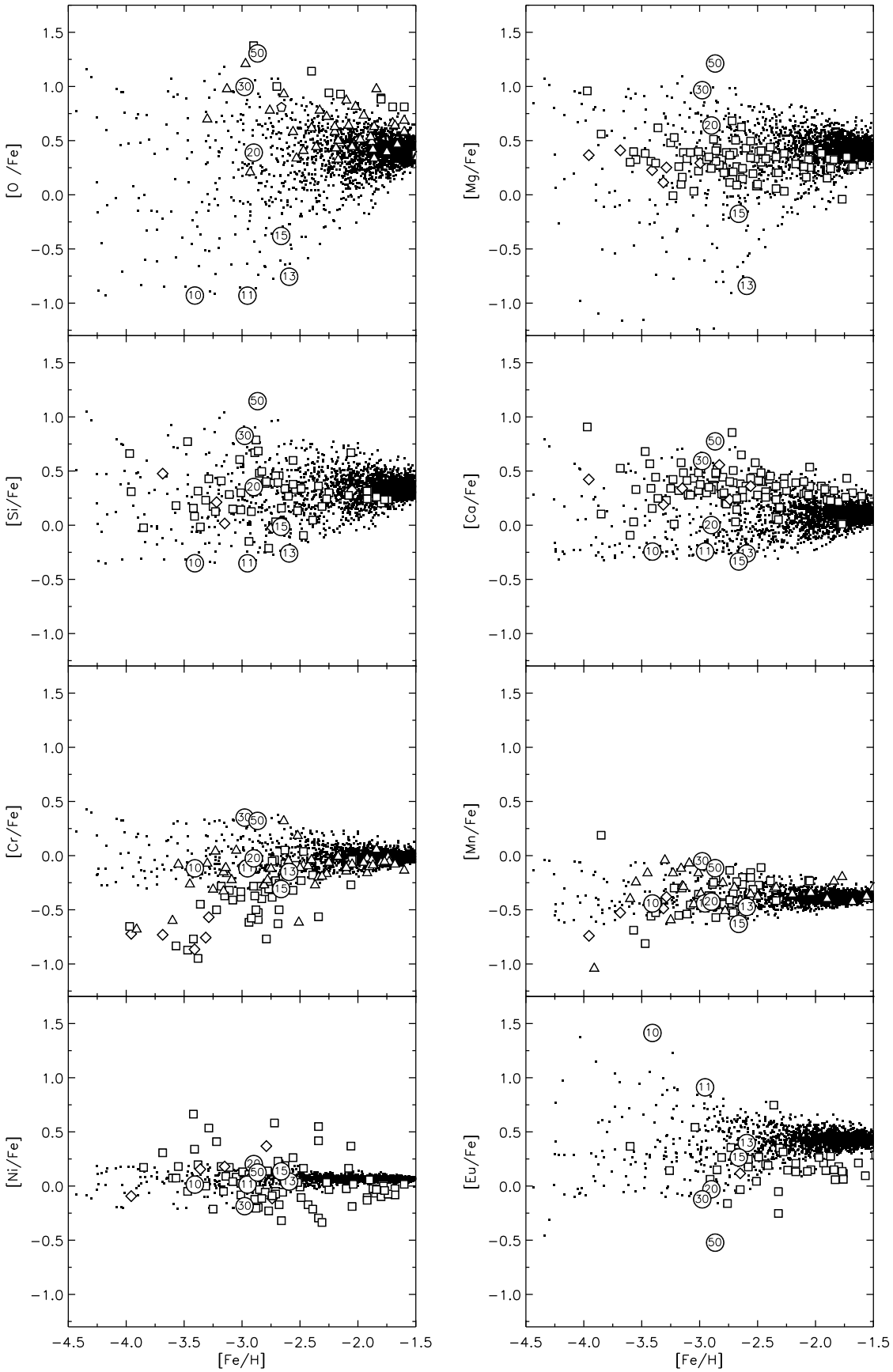

Fig. 2. Element-to-iron ratio [El/Fe] of O, Mg, Si, Ca, Cr, Mn, Ni and Eu. Open circles depict [El/Fe] ratios of SN II models of the given progenitor mass. Small filled squares represent model stars, open symbols show observed stars.